MODEL REDUCTION FOR GUST LOAD ANALYSIS OF FREE-FLYING AIRCRAFT

G. Pagliuca[1], P. Bekemeyer[1], R. Thormann[1], S. Timme[1]

[1]School of Engineering, University of Liverpool, Liverpool, L69 3GH, UK

Keywords: model reduction, computational fluid dynamics, flight dynamics

Abstract: The coupling of computational fluid dynamics and rigid body dynamics promises enhanced multidisciplinary simulation capability for aircraft design and certification. Industrial application of such coupled simulations is limited however by computational cost. In this context, model reduction can retain the fidelity of the underlying model while decreasing the computational effort. A model reduction technique is presented herein based on modal decomposition and projection of the non-linear residual function. Flight dynamics eigenmodes are obtained with an operator-based identification procedure which is capable of calculating these global modes of the coupled Jacobian matrix also for an industrial use case with nearly 50 million degrees-of-freedom. Additional modes based on proper orthogonal decomposition to describe the aerodynamic response due to gust encounter are combined with the eigenmode basis. Results are presented for initial disturbance analysis using flight dynamics modes only and for gust encounter simulations using the combined modal basis. Overall, the reduced model is capable of predicting the full order results accurately.

1 INTRODUCTION

Multidisciplinary simulations involving flight dynamics and aerodynamics represent the next step towards a reduction of in-flight testing requirements [1] and improved accuracy for the aircraft design and certification process [2]. Nowadays, industrial practice still adopts corrected linear potential methods as aerodynamic models while various solutions were proposed to account for free-flight effects [3, 4]. These models offer low fidelity at affordable computational cost. Their validity is extended to transonic flows by means of correction procedures involving tailored expertise which nullify the efforts for a quick, automated load evaluation. Also, the accuracy of these corrected methods deteriorates towards edge-of-envelope flights conditions.

Application in the transonic regime requires high-fidelity aerodynamics provided by computational fluid dynamics (CFD) which is capable of describing non-linear flow phenomena like shock waves and large separations. However, a higher computational cost has to be paid. The CFD solver is usually coupled with a structural solver while the flight dynamics behaviour is prescribed [5]. An extension to properly coupled simulations requires the flight dynamics unknowns, which depend on the most recent values of aerodynamic forces and vice versa, to be calculated at each time-step. In addition, the system can be subject to external disturbance such as gusts. Recently, it was shown that flight dynamics effects cannot be neglected in high-fidelity gust loads analysis [6]. Comparison between CFD and tools currently used in industrial practice highlighted the limitations of the latter. However, a wider adoption of CFD aerodynamics is limited by computational resources. A first cost reduction has already been demonstrated

using linearised frequency domain (LFD) formulations for both aerodynamic response only [7] and fluid-structure coupled simulations [8, 9]. Nevertheless, faster methods that keep the high fidelity in transonic flow are still desirable.

Reduced order modelling offers a reduction in computational cost while retaining the fidelity of underlying methods. High-fidelity aerodynamics is typically represented by a generalised aerodynamic force matrix and the response is then obtained by integrating the low-dimensional modal equations in time [10]. Another possible approach operates on the coupled system as a whole. It manipulates the full order, coupled, non-linear residual function expanded in a Taylor series with a projection on an appropriate modal basis resulting in a monolithic reduced model [11]. The projection method produces a versatile reduced model which facilitates a comprehensive study of the coupled system. Previous application includes the simulation of coupled structural and aerodynamic systems using linear potential aerodynamics for gust encounter analysis and robust control [11, 12]. An extension to CFD is possible by calculating modes for the projection using the Schur complement method [13]. This was applied to a flexible aircraft for aeroelastic analyses in transonic flow in [9] while the feasibility of including free-flight effects was shown for a two-dimensional test case in [14]. This formulation can also be used for structural non-linearities [15] and might be expanded to account for aerodynamic non-linearities leading to limit cycle oscillations [16]. An extension for gust responses including additional modes from proper orthogonal decomposition is available [17, 18]

In this paper, the model reduction technique based on modal projection is applied to a large civil aircraft flying in the transonic regime. The reduced order model (ROM) uses eigenmodes of the coupled system which are related to flight dynamics modes [19, 20]. They correspond to a few eigenpairs of the coupled Jacobian matrix. Calculating the complete eigenspectrum of the coupled system and applying a trial-and-error approach to find the flight dynamics eigenpairs is prohibitive even for small-sized test cases. An operator-based identification procedure is proposed instead to compute these specific eigenpairs directly. The procedure starts with computing the generalised aerodynamic force matrices with LFD methods and continues with the tracing of eigenpairs. Particular care is needed when computing flight dynamics modes. They arise from the in-vacuum rigid body modes which are all characterised by zero frequency and damping. As a result, the position of flight dynamics eigenvalues in the complex plane completely depends on the coupling between fluid and rigid body modes. The reduced model formulation is exploited for initial disturbance analyses and for gust encounter simulations. The aerodynamic subsystem is sampled to obtain complex-valued responses to sinusoidal gusts. Proper orthogonal decomposition (POD) is applied to the samples resulting in POD modes. These are then added to the reduced model in order to reproduce accurately the gust response.

The paper proceeds in Section 2 with a description of the theoretical formulation. The reduction method is derived and the identification procedure is reported. The application of POD for gust disturbance is described thereafter while an overview of the numerical approach is given in Section 3. In Section 4 results are presented for a large civil aircraft. Reference solutions are provided by the full order model implemented within the FlowSimulator framework [21]. It is based on Reynolds-averaged Navier–Stokes (RANS) aerodynamics while three-dimensional rigid body dynamics is taken into account with a modal approach. First, results are shown using flight dynamics modes only. Subsequently, these modes are combined with POD modes describing the aerodynamic response to gust disturbances. Results are presented for gust encounter simulations of a free-flying large civil aircraft.

2 NUMERICAL APPROACH

2.1 Full order model and model reduction

Denoting $\boldsymbol{w}_r$ as the vector containing n_r flight dynamics unknowns and $\boldsymbol{R}_r$ as the corresponding non-linear residual function, the equations of motion are formulated as a first order ordinary differential equation in time t,

$$\frac{\mathrm{d}\boldsymbol{w}_r}{\mathrm{d}t} = \boldsymbol{R}_r(\boldsymbol{w}_f, \boldsymbol{w}_r) \tag{1}$$

with the vector $\boldsymbol{w}_f$ containing the n_f fluid unknowns. Specifically, the residual vector $\boldsymbol{R}_r$ is written as

$$\boldsymbol{R}_r(\boldsymbol{w}_f, \boldsymbol{w}_r) = \boldsymbol{f}_e(\boldsymbol{w}_r) + \boldsymbol{f}_a(\boldsymbol{w}_f, \boldsymbol{w}_r) \tag{2}$$

with $\boldsymbol{f}_a$ representing aerodynamic forces. The formulation of the vector function $\boldsymbol{f}_e$ depends on the underlying flight dynamics model. In general, it contains information about mass distribution and includes external forces such as gravity. The non-linear equations describing aerodynamics are similarly written in a semi-discrete form as

$$\frac{\mathrm{d}\boldsymbol{w}_f}{\mathrm{d}t} = \boldsymbol{R}_f(\boldsymbol{w}_f, \boldsymbol{w}_r, \boldsymbol{u}_d) \tag{3}$$

where $\boldsymbol{R}_f$ is the non-linear residual corresponding to the fluid unknowns and $\boldsymbol{u}_d$ represents a possible external disturbance such as gusts. Denoting $\boldsymbol{w} = [\boldsymbol{w}_f^T, \boldsymbol{w}_r^T]^T$ as the vector of unknowns of the coupled system, the state-space equations of dimension $n = n_f + n_r$ can be combined as

$$\frac{\mathrm{d}\boldsymbol{w}}{\mathrm{d}t} = \boldsymbol{R}(\boldsymbol{w}, \boldsymbol{u}_d) \tag{4}$$

where $\boldsymbol{R}$ is the corresponding coupled non-linear residual vector.

The system in Eq. (4) is expanded in a first order Taylor series around an equilibrium state with $\boldsymbol{R}(\boldsymbol{w}_0, \boldsymbol{u}_{d0}) = 0$,

$$\boldsymbol{R}(\boldsymbol{w}, \boldsymbol{u}_d) = A\,\widetilde{\boldsymbol{w}} + \frac{\partial \boldsymbol{R}}{\partial \boldsymbol{u}_d}\widetilde{\boldsymbol{u}}_d + O\left(|\widetilde{\boldsymbol{w}}|^2, |\widetilde{\boldsymbol{u}}_d|^2\right) \tag{5}$$

where $\boldsymbol{w}(t) = \boldsymbol{w}_0 + \widetilde{\boldsymbol{w}}(t)$ and accordingly $\boldsymbol{u}_d(t) = \boldsymbol{u}_{d0} + \widetilde{\boldsymbol{u}}_d(t)$. The Jacobian matrix A of dimension $n \times n$ is partitioned into blocks

$$A = \begin{pmatrix} A_{ff} & A_{fr} \\ A_{rf} & A_{rr} \end{pmatrix} \tag{6}$$

with

$$A_{ff} = \frac{\partial \boldsymbol{R}_f}{\partial \boldsymbol{w}_f} \qquad A_{fr} = \frac{\partial \boldsymbol{R}_f}{\partial \boldsymbol{w}_r} \qquad A_{rf} = \frac{\partial \boldsymbol{f}_a}{\partial \boldsymbol{w}_f} \qquad A_{rr} = \frac{\partial \boldsymbol{f}_e}{\partial \boldsymbol{w}_r} + \frac{\partial \boldsymbol{f}_a}{\partial \boldsymbol{o}}\frac{\partial \boldsymbol{o}}{\partial \boldsymbol{w}_r} \tag{7}$$

The diagonal blocks A_{ff} and A_{rr} are fluid and flight dynamics Jacobian matrices, respectively, whereas the off-diagonal blocks describe the coupling terms. Specifically, the matrix A_{rf} links aerodynamic forces to fluid unknowns and A_{fr} represents fluid excitation due to the flight dynamics degrees-of-freedom. The term $\frac{\partial \boldsymbol{f}_a}{\partial \boldsymbol{o}}$ relates a change of aerodynamic forces to a rotation of surface normals $\boldsymbol{o}$ while keeping the flow variables fixed.

Two LFD formulations are extensively used in the paper to obtain aerodynamic responses. The first is derived considering the homogeneous form of Eq. (5) with $\widetilde{\boldsymbol{u}}_d = 0$. The partitioning in

Eq. (6) is applied and the transformation to frequency domain is obtained with $\widetilde{\boldsymbol{w}}_f(t) = \hat{\boldsymbol{w}}_f e^{i\omega t}$ and $\widetilde{\boldsymbol{w}}_r(t) = \hat{\boldsymbol{w}}_r e^{i\omega t}$. Isolating the fluid unknowns leads to

$$\left(A_{ff} - i\omega I\right)\hat{\boldsymbol{w}}_f = -A_{fr}\hat{\boldsymbol{w}}_r \tag{8}$$

This equation is useful to compute the motion-induced aerodynamic responses to harmonic excitation in the flight dynamics degrees-of-freedom. The second formulation targets aerodynamic responses to external, sinusoidal excitations with $\hat{\boldsymbol{u}}_d = \widetilde{\boldsymbol{u}}_d e^{i\omega t}$, resulting in

$$\left(A_{ff} - i\omega I\right)\hat{\boldsymbol{w}}_f = -\frac{\partial \boldsymbol{R}}{\partial \boldsymbol{u}_d}\hat{\boldsymbol{u}}_d \tag{9}$$

and it will be used to sample the gust-induced aerodynamic response.

The model reduction is performed by projecting the Taylor series in Eq. (5) on a smaller modal basis. The bases Φ and Ψ are built by choosing m appropriate modes,

$$\Phi = \left(\ \boldsymbol{\phi}^{(1)}, \quad \boldsymbol{\phi}^{(2)}, \quad \ldots, \quad \boldsymbol{\phi}^{(m)}\ \right) \qquad \text{and} \qquad \Psi = \left(\ \boldsymbol{\psi}^{(1)}, \quad \boldsymbol{\psi}^{(2)}, \quad \ldots, \quad \boldsymbol{\psi}^{(m)}\ \right) \tag{10}$$

scaled to satisfy the conditions

$$\langle \boldsymbol{\phi}^{(i)}, \boldsymbol{\phi}^{(i)} \rangle = 1 \qquad \text{and} \qquad \langle \boldsymbol{\psi}^{(i)}, \boldsymbol{\phi}^{(i)} \rangle = 1 \qquad\qquad \forall i \in [1, m] \tag{11}$$

where the Hermitian inner product $\langle \boldsymbol{x}, \boldsymbol{y} \rangle$ is defined as $\bar{\boldsymbol{x}}^T \boldsymbol{y}$. The model reduction is performed with the variable transformation

$$\widetilde{\boldsymbol{w}} = \Phi \boldsymbol{z}, \quad \boldsymbol{z} \in \mathbb{C}^m \tag{12}$$

and pre-multiplying with the left modal basis Ψ. Including complex conjugate pairs in the modal basis in Eq. (10) gives a real-valued vector $\widetilde{\boldsymbol{w}}$ in Eq. (12). The reduced order model is then expressed as

$$\bar{\Psi}^T \Phi \frac{\mathrm{d}\boldsymbol{z}}{\mathrm{d}t} = \bar{\Psi}^T A \Phi\, \boldsymbol{z} + \bar{\Psi}^T \frac{\partial \boldsymbol{R}}{\partial \boldsymbol{u}_d} \widetilde{\boldsymbol{u}}_d \tag{13}$$

and integrated in time to obtain time-domain response $\boldsymbol{z}(t)$. Assuming harmonic excitation $\widetilde{\boldsymbol{u}}_d = \hat{\boldsymbol{u}}_d e^{i\omega t}$ and harmonic response $\boldsymbol{z}(t) = \hat{\boldsymbol{z}} e^{i\omega t}$, Eq. (13) can also be rewritten in frequency domain,

$$\bar{\Psi}^T \left(A - i\omega I\right) \Phi \hat{\boldsymbol{z}} = -\bar{\Psi}^T \frac{\partial \boldsymbol{R}}{\partial \boldsymbol{u}_d}\ \hat{\boldsymbol{u}}_d \tag{14}$$

Exploiting Eq. (14) is more convenient for responses to sinusoidal external disturbances while Eq. (13) leads to the same results. Solutions for non-harmonic excitations are obtained by expanding the input signal in Fourier series and applying superposition of results.

The modal bases in Eq. (10) must be built from modes representing the dominating system behaviour. A procedure, named operator-based modal identification, is described in the following and applied to calculate these modes. In addition, the evaluation of modes describing the aerodynamic subsystem for gust simulations is presented thereafter.

2.2 Operator-based modal identification

The system in Eq. (4) is expanded by means of Eq. (5) and translated into Laplace domain with complex-valued variable λ. The external disturbance $\boldsymbol{u}_d$ is zero for operator-based identification. This leads to the direct and adjoint eigenvalue problems,

$$\left(A - \lambda^{(i)}I\right)\boldsymbol{\phi}^{(i)} = 0 \qquad \text{and} \qquad \left(A^T - \lambda^{(i)}I\right)\bar{\boldsymbol{\psi}}^{(i)} = 0 \qquad \forall i \in [1, m] \qquad (15)$$

where $(\lambda^{(i)}, \boldsymbol{\phi}^{(i)})$ and $(\lambda^{(i)}, \boldsymbol{\psi}^{(i)})$ are the corresponding eigenpairs. A subset of m direct and adjoint eigenvectors related to flight dynamics degrees-of-freedom is included in the modal bases for the model reduction. Note that in this case the conditions in Eq. (11) are satisfied due to the bi-orthonormality of eigenvectors,

$$\langle \boldsymbol{\psi}^{(j)}, \boldsymbol{\phi}^{(i)} \rangle = \delta_{ij} \qquad \text{and} \qquad \langle \boldsymbol{\psi}^{(j)}, \bar{\boldsymbol{\phi}}^{(i)} \rangle = 0 \qquad \forall i, j \in [1, m] \qquad (16)$$

where δ_{ij} is the Kronecker delta.

The small eigenvalue problem of dimension n_r resulting from the flight dynamics part of the direct eigenproblem in Eq. (15) is

$$\left[\left(A_{rr} - \lambda^{(i)}I\right) - \beta A_{rf} \left(A_{ff} - \lambda^{(i)}I\right)^{-1} A_{fr} \right]\boldsymbol{\phi}_r^{(i)} = S(\lambda^{(i)})\boldsymbol{\phi}_r^{(i)} = 0 \qquad (17)$$

where $S(\lambda^{(i)})$ is the spectral Schur complement of A with respect to flight dynamics degrees-of-freedom. An artificial weighting factor β is introduced to gradually add the coupling effect. Newton's method solving for $(\lambda^{(i)}, \boldsymbol{\phi}_r^{(i)})$ is used to trace the evolution of the rigid body degrees-of-freedom starting from zero frequency at $\beta = 0$ to the coupled eigenvalue at $\beta = 1$. The corresponding fluid part $\boldsymbol{\phi}_f^{(i)}$ of the eigenvector is calculated for the converged solution $(\lambda^{(i)}, \boldsymbol{\phi}_r^{(i)})$ at $\beta = 1$ by solving

$$\left(A_{ff} - \lambda^{(i)}I\right)\boldsymbol{\phi}_f^{(i)} = -A_{fr}\boldsymbol{\phi}_r^{(i)} \qquad (18)$$

The computationally expensive part of Eq. (17) is the repeated evaluation of the interaction term $A_{rf}\left(A_{ff} - \lambda^{(i)}I\right)^{-1} A_{fr}$ depending on the solution $\lambda^{(i)}$. For small-sized problems, this matrix can be computed with direct solvers whereas iterative solvers have to be applied for industrial test cases [22]. This can lead to convergence problems since the eigenspectrum of the system can contain up to millions of eigenvalues and the flight dynamics eigenvalue might be within the cloud of aerodynamic modes. A Taylor expansion for $\lambda = \lambda_0 + \lambda_\epsilon$ was proposed in [8, 13] to alleviate this problem and speed-up the tracing.

The adjoint eigenvalue problem, the solution of which is needed for the model reduction, is equivalently formulated as

$$\left\{ \left(A_{rr}^T - \lambda^{(i)}I\right) - \beta \left[A_{rf} \left(A_{ff} - \lambda^{(i)}I\right)^{-1} A_{fr}\right]^T \right\}\bar{\boldsymbol{\psi}}_r^{(i)} = 0 \qquad (19)$$

while the fluid part of the left eigenvector is then calculated by solving the adjoint problem corresponding to Eq. (18).

The derivation so far has previously been described as Schur complement method. The relation to more classical analysis via pre-computation of an interaction matrix is apparent. Substituting the definition of A_{rf} into Eq. (17), the interaction term is expressed as

$$A_{rf} \left(A_{ff} - \lambda^{(i)}I\right)^{-1} A_{fr} = \frac{\partial \boldsymbol{f}_a}{\partial \boldsymbol{w}_f} \left(A_{ff} - \lambda^{(i)}I\right)^{-1} A_{fr} \qquad (20)$$

The term $\left(A_{ff} - \lambda^{(i)}I\right)^{-1} A_{fr}$ is associated in Eq. (8) with the response of the fluid unknowns to excitations in the flight dynamics degrees-of-freedom,

$$\frac{\partial \boldsymbol{f}_a}{\partial \boldsymbol{w}_f} \left(A_{ff} - \lambda^{(i)}I\right)^{-1} A_{fr} = \frac{\partial \boldsymbol{f}_a}{\partial \boldsymbol{w}_f}\frac{\partial \boldsymbol{w}_f}{\partial \boldsymbol{w}_r} = \frac{\partial \boldsymbol{f}_a}{\partial \boldsymbol{w}_r} = Q \tag{21}$$

Thus, the matrix Q describes the complex-valued transfer function relating rigid motions to the aerodynamic forces [23, 24]. The direct and adjoint eigenvalue problems in Eqs. (17) and (19) are then rewritten as

$$\left[\left(A_{rr} - \lambda^{(i)}I\right) + \beta Q\right]\boldsymbol{\phi}_r^{(i)} = 0 \qquad\qquad \left[\left(A_{rr}^T - \lambda^{(i)}I\right) + \beta Q^T\right]\bar{\boldsymbol{\psi}}_r^{(i)} = 0 \tag{22}$$

The matrix Q is pre-computed for a finite number of harmonic motions with values of damping and frequency corresponding to real and imaginary pairs in the complex plane. Interpolation techniques are used to calculate values for points not sampled. The latter equations are identical to Eqs. (17) and (19), if Q is computed for each point in the complex plane.

A simplification arises by neglecting the damping during the computation of the aerodynamic influence, similar to the p-k method [25]. As a consequence, the matrix Q would depend on frequency only and pre-computed for simple harmonic motions.

2.3 Proper orthogonal decomposition

The snapshot method [26] is adopted to obtain modes describing the response of the aerodynamic subsystem subject to sinusoidal gust disturbances. A snapshot matrix S of dimension $n_f \times 2m_{\text{POD}}$ is obtained by combining m_{POD} solutions of Eq. (9) and their complex-conjugates for frequencies in the range of interest. Producing the snapshots is the computationally expensive part of the method since m_{POD} complex-valued linear systems with leading dimension n_f need to be solved. POD is then applied to the snapshot matrix S which leads to the calculation of POD modes. The procedure is applied to gust excitations as described in detail in [27].

2.4 Combination of modal bases

POD modes, assembled as columns of the matrix Φ_{POD}, are padded with zeros to account for the missing n_r entries and included in the matrices Φ and Ψ in Eq. (10). The joint modal bases are now defined as

$$\Phi = \left(\ \Phi_{\text{EMD}}, \quad \Phi_{\text{POD}}\ \right) \qquad \text{and} \qquad \Psi = \left(\ \Psi_{\text{EMD}}, \quad \Psi_{\text{POD}}\ \right) \tag{23}$$

with $\Psi_{\text{POD}} = \Phi_{\text{POD}}$, and Φ_{EMD} and Ψ_{EMD} containing the direct and adjoint eigenvectors from the operator-based identification, respectively. This method has previously been applied to a flexible structure for gust encounter simulations and more details about the technique are available in [18]. The first application to flight dynamics is presented in the current paper.

3 NUMERICAL ASPECTS

Aerodynamics forces are calculated with the DLR-TAU code which is widely used in the European aerospace sector and validations of the code is available in the literature for steady [28, 29] and unsteady cases [29, 30]. The RANS equations in conjunction with the Spalart-Allmaras turbulence model [31] are solved. Inviscid fluxes are discretised applying a central scheme

with scalar artificial dissipation of Jameson, Schmidt and Turkel [32]. Exact gradients used for viscous and source terms are computed using the Green-Gauss approach. Steady-state solutions are obtained using backward Euler method with lower-upper Symmetric-Gauss-Seidel iterations [33] and local time-stepping. Convergence is accelerated by applying a 2v multigrid scheme. Unsteady simulations are performed with a dual-stepping method combined with a second order backward Euler scheme. The LFD formulation used for the calculation of the interaction matrix is based on a first-discretise-then-linearise, matrix-forming approach with an analytical, hand-differentiated Jacobian matrix. A generalised conjugate residual solver with deflated restarting is used to solve arising linear systems [22]. Preconditioning is provided with an incomplete lower-upper factorisation of the Jacobian matrix with zero level of fill-in applied. Gusts are introduced with the field velocity method [34] for which an artificial mesh velocity term is added to the CFD equations.

Rigid body dynamics is modelled with a modal approach,

$$M\ddot{\boldsymbol{\eta}} = \Xi^T \boldsymbol{f} \tag{24}$$

where $\boldsymbol{\eta}$ is the vector of modal coordinates and M is modal mass matrix corresponding to the mass-normalised rigid body modes. Aerodynamic forces and gravity are included in $\boldsymbol{f}$. Generalised aerodynamic forces (GAF) are obtained with a multiplication by the matrix Ξ which contains the mode shapes as columns. This system is integrated using a β-Newmark scheme [35]. To be consistent with Eq. (1) for the purpose of model reduction, the second order system in Eq. (24) is written in first order form with $\boldsymbol{w}_r = [\boldsymbol{\eta}^T, \dot{\boldsymbol{\eta}}^T]^T$.

The coupled problem is implemented within the FlowSimulator framework [21]. Aerodynamics and modal rigid dynamics are solved separately and data is exchanged on a subiteration level. At each sub-iteration, the generalised forces are computed and the set of modal equations is solved. In turn, the CFD mesh is deformed with radial basis function interpolation [36] according to modal displacements and aerodynamic forces recomputed. The iterative process at each time step is stopped when the norm of the update of the generalised forces is smaller than 10^{-4}.

A set of 6 rigid body modes is used when solving Eq. (24). These modes resulting from an in-vacuum eigenvalue analysis of finite element model in Nastran are a combination of translations and rotations in the three-dimensional space. This becomes clear in Fig. 1 where two representative mode shapes are shown. For example, the mode in Fig. 1(a) is composed mainly of yaw rotation but a translational component is visible. Similarly, mode 4 in Fig. 1(b) shows roll rotation alongside vertical translation. Although this does not represent an issue for the numerical model, a link to the physical quantities traditionally adopted for longitudinal and lateral flight dynamics is not immediately available. A possible solution is to perform a transformation of modal basis. An new set of 6 pure translational and rotational modes Υ is created by prescribing translations of 1 m in each of the 3 directions and rotations of 1 deg around each of the 3 axes according to the sign convention usually adopted in flight dynamics [20, 37] and shown in Fig. 2. Denoting the horizontal, lateral and vertical translation as x_I, y_I and z_I, respectively, and the roll, pitch and yaw rotations as ϕ, θ and ψ, the vector $\boldsymbol{\chi} = [x_I, y_I, z_I, \phi, \theta, \psi]^T$ contains the modal amplitudes for this new set of modes. Since the same physical rigid motion $\boldsymbol{x}$ can now be obtained with those two sets of modes, we can write

$$\Upsilon \boldsymbol{\chi} = \boldsymbol{x} = \Xi \boldsymbol{\eta} \tag{25}$$

Mapping modal displacement $\boldsymbol{\eta}$ to physical quantities $\boldsymbol{\chi}$ is achieved with

$$\boldsymbol{\chi} = \left(\Upsilon^T \Upsilon\right)^{-1} \Upsilon^T \Xi \boldsymbol{\eta} = T \boldsymbol{\eta} \tag{26}$$

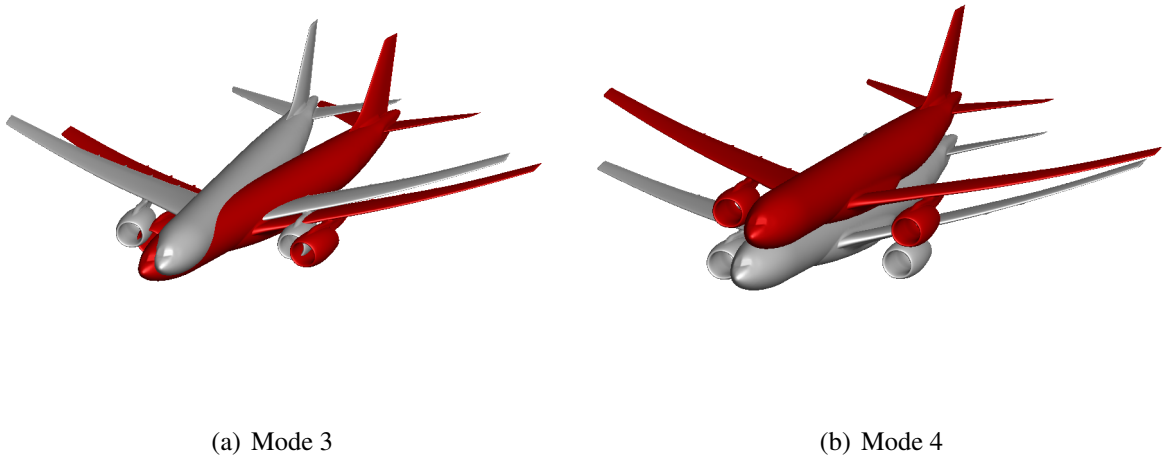(a) Mode 3   (b) Mode 4

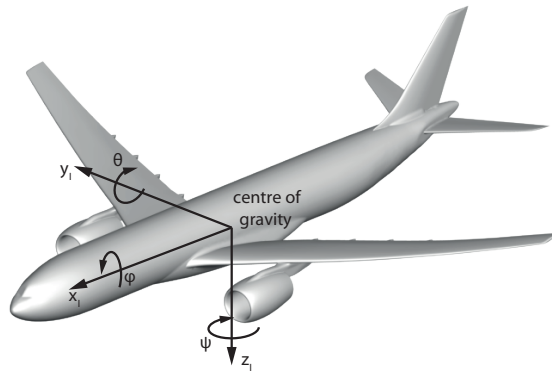Figure 1: Mode shapes for two of the modes accounting for the rigid body dynamics.

Figure 2: Sign convention used to present results with physical quantities.

where a 6×6 transformation matrix $T = \left(\Upsilon^T \Upsilon\right)^{-1} \Upsilon^T \Xi$ is defined. The transformation matrix T is precomputed once and used in the following to provide physical insights about the system.

4 RESULTS

Results are presented for a large civil aircraft in cruise condition flying at 10 km altitude, Mach number of 0.85 and Reynolds number of about 49 millions. The mesh for CFD calculations consists of nearly 8 millions points with a far field at 77 wing chords. The steady state solution results from an iterative trimming procedure based on the Broyden method [38]. Conditions for straight and level flight provide target values for lift and moment while elastic deformations are taken into account by including 94 elastic modes in the procedure. The reference point for rotation is the centre of mass. Angle of attack and horizontal tail rotation are updated iteratively to meet the requirements. Thrust balances drag at the equilibrium and its orientation is assumed horizontal at all time. The CFD mesh is deformed at each iteration to account for elastic deformation. The pressure coefficient for the resulting steady state is shown in Fig. 3. A shockwave is clearly visible on the upper surface of the wing while the horizontal tail is shock free. These non-linearities are retained in the reduced model which describes the variations of fluid and flight dynamics unknowns around this trimmed solution.
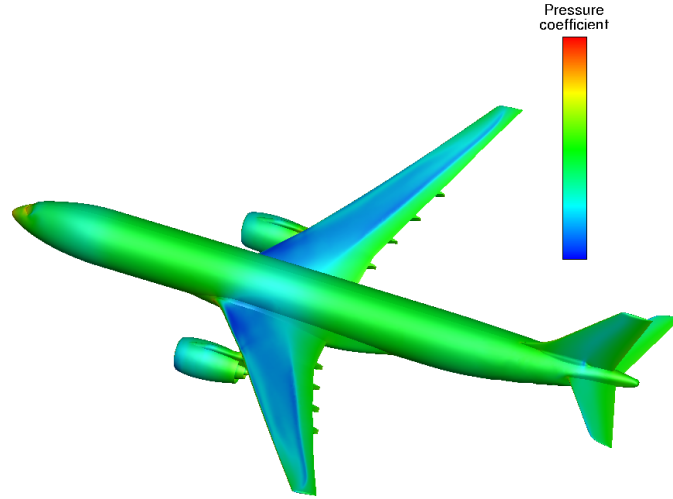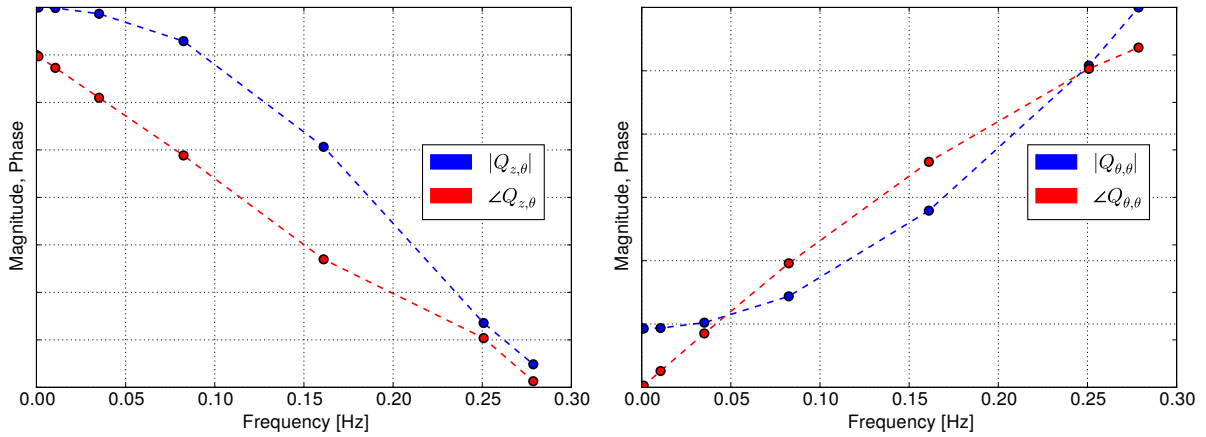
Figure 3: Steady state solutions as resulting from the trimming procedure.

(a) Entry relating the vertical translation GAF to sinusoidal pitch rotation

(b) Entry relating the pitch rotation GAF to pitch rotation

Figure 4: Magnitude and phase of two representative entries of the GAF matrix Q.

The operator-based identification procedure is described next for flight dynamics modes. The geometry resulting from the elastic trimming is now frozen and the system assumed to evolve rigidly without any additional elastic deformation. The 6×6 GAF matrix Q in Eq. (22) was precomputed in the frequency domain. For each of the 6 rigid body modes, the right-hand side of Eq. (8) was produced using central finite differences and the linear system solved at the specified reduced frequencies. This corresponds to calculating the aerodynamic responses to sinusoidal rigid motions. The complex-valued flow solutions were then projected onto the rigid body modes providing the frequency response function relating the sinusoidal excitations to GAFs for the 6 modes. The result of these calculations are complex-valued GAF matrices computed at 7 positive values of ω spaced according to a power law of 3 in the reduced frequency range $[0, 0.05]$. Magnitude and phase of two representative entries of Q are depicted in Fig. 4 as function of frequency using Eq. (26) and the sign convention in Fig. 2 to provide physical quantities.

The tracing in Eq. (22) leading to the flight dynamics parts of the eigenvectors of the coupled system is performed using Newton's method and cubic Hermite spline interpolation is adopted to evaluate Q at frequencies not sampled. A relaxation parameter of 0.8 is adopted for the New-
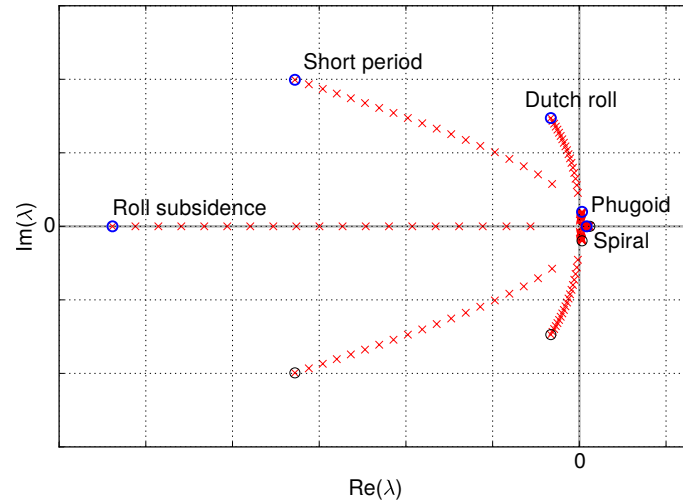
Figure 5: Eigenspectrum showing flight dynamics eigenvalues resulting from the tracing.

ton solver. The derivative $\frac{\mathrm{d}Q}{\mathrm{d}\lambda} \approx \frac{\partial Q}{\partial \omega}$ is used in the implementation to accelerate the convergence and it is calculated using central finite differences with $\epsilon = 1 \times 10^{-8}$. The procedure starts at a small value of $\beta = 0.15$ with the calculation of the initial guess needed by the Newton solver. Eigensolutions of the small system in Eq. (22) are calculated assuming $Q = Q(\omega = 0)$ with direct methods implemented in the `eig` function in MATLAB. It can be noticed that the entries of $Q(0)$ correspond to stability derivatives which are usually adopted to investigate the behaviour of flight dynamics systems. The eigensolutions of this simplified problem are employed as initial guess for the tracing which is composed of two loops. The outer loop increases the value of β gradually in 19 steps until the coupling of flight dynamics and aerodynamics is fully taken into account at $\beta = 1$. At each value of β, the inner loop is started by the Newton solver which iterates until the norm of the residual vector is below 1×10^{-13}. The converged solution is then returned to the outer loop which will use it as initial guess to seek the eigensolution for the next β value. Calculation of eigenpairs corresponding to negative reduced frequencies can be avoided since they are not needed. The fluid parts of eigenvectors are then computed with Eq. (18) assuming $\Re(\lambda) = 0$, to employ consistent aerodynamics.

The eigenvalues resulting from the tracing are shown in the complex plane in Fig. 5. Their evolution from the rigid body modes characterised by zero frequency and damping is clearly visible and due to the gradual inclusion of aerodynamics. The tracing procedure shows that these eigenvalues move to locations in the complex plane corresponding to real numbers as well as complex conjugate pairs and a physical interpretation can be given in terms of dynamic stability modes [20]. They are identified using their eigenvector components in addition to frequency information available in literature. For longitudinal dynamics, two periodic modes were expected, namely short period and phugoid. The short period corresponds to the complex-conjugate pair with the highest reduced frequency. The motion it describes is composed of pitch rotation and vertical velocity. Regarding the phugoid which is characterised by varying pitch rotation and horizontal speed, it must be noted that some simplifications are made in the full model since the thrust orientation does not follow the pitch rotation. Although this does not fully reflect the physical behaviour, the phugoid mode can be found close to the origin having a very long period and small damping. Regarding lateral dynamics, three modes were expected specifically Dutch roll, spiral and roll subsidence modes. The first one corresponds to the complex conjugate pair with the second highest reduced frequency. It lies in the same reduced frequency range of the short period mode but it is completely unrelated to longitudinal

10

(a) Response in the pitch rotation

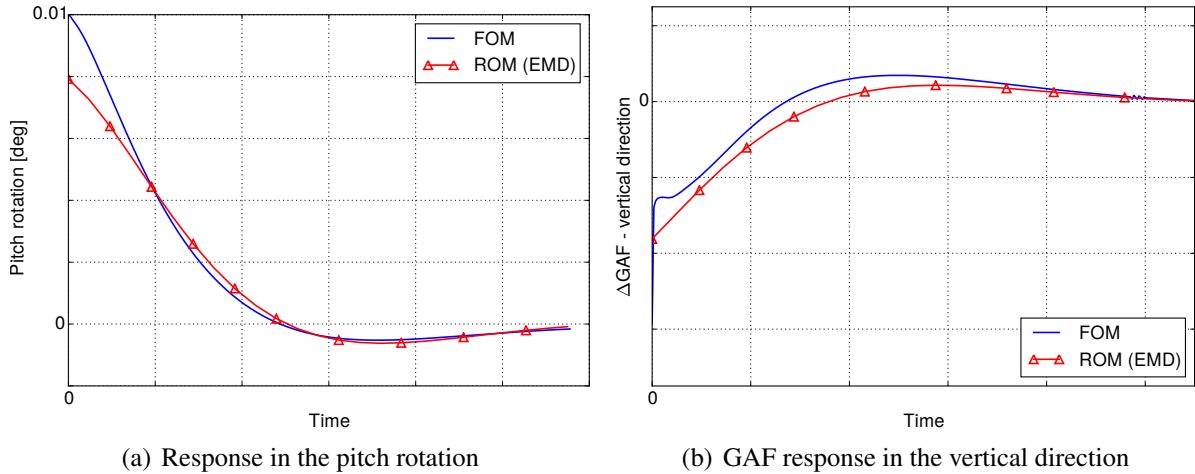(b) GAF response in the vertical direction

Figure 6: Results for an initial disturbance of 0.01 degree in the pitch rotation. ROM includes flight dynamics modes only.

dynamics since it is mainly composed of roll and yaw rotations. The roll mode is stable with a negative real part and zero reduced frequency. Conversely, real-valued spiral mode is unstable. The nature of the remaining eigenpairs is still under investigation. Their eigenvectors represent absolute translations which do not affect the aerodynamic response [39] and for which the eigenvalues are supposed to be zero. However, the corresponding eigenvalues are small real numbers located around the origin and their values could be affected by numerical inaccuracies.

The tracing procedure is performed for adjoint and direct problems so that modal bases in Eq. (10) were assembled. The reduced model was first used to perform initial disturbance analysis and results are shown in Fig. 6 for a disturbance in the pitch rotation of 0.01 degrees. Overall, full and reduced model show a stable response as expected from the real part of the longitudinal eigenvalues. In Fig. 6(a) the pitch rotation is depicted. Initial conditions are not fully reconstructed by the reduced model and this can be interpreted as information lost when reducing the model from about 48 million to 12 degrees-of-freedom. The trend for pitch rotation is thereafter captured accurately by the reduced model with results converging to the full order ones. In Fig. 6(b) a similar trend is shown for the GAF in the vertical direction. The full order model GAF shows an initial jump from a zero value followed by a slow recovery. Apart from the discrepancy in the initial conditions already discussed for the pitch rotation, the ROM results match the full order response. Summarising, the reduced model containing 12 flight dynamics modes, specifically 3 complex-conjugate pairs and 6 real-valued eigenvectors, is able to reproduce results for initial disturbance analyses.

The model is then expanded to account for external gust disturbances by introducing the term $\frac{\partial R}{\partial u_d}$ in Eq. (13) and defining the shape of the travelling gust with the vector $\widetilde{u}_d$. Results for a '1-cos' gust with wavelength $L_g = 116$ m and two gust amplitudes V_{g_z} are presented in Fig. 7. Two curves are shown for the full order model. The first corresponds to a gust disturbance acting linearly ($V_{g_z} = 0.01\%$ of free-stream velocity) whereas the second one represents a gust amplitude as prescribed by EASA regulations for the given gust length ($V_{g_z} = 6.1\%$ of free-stream velocity). Although ROM results should be compared to the linear model, including results for the regulation gust helps highlighting non-linear effects. Both reference solutions show an oscillation for the pitch rotation GAF in Fig. 7(a). This is due to the alteration in pitching moment brought by the disturbance which is followed by a response from the stable system. Non-linear effects alter the peak values and accelerate the response decay as shown by
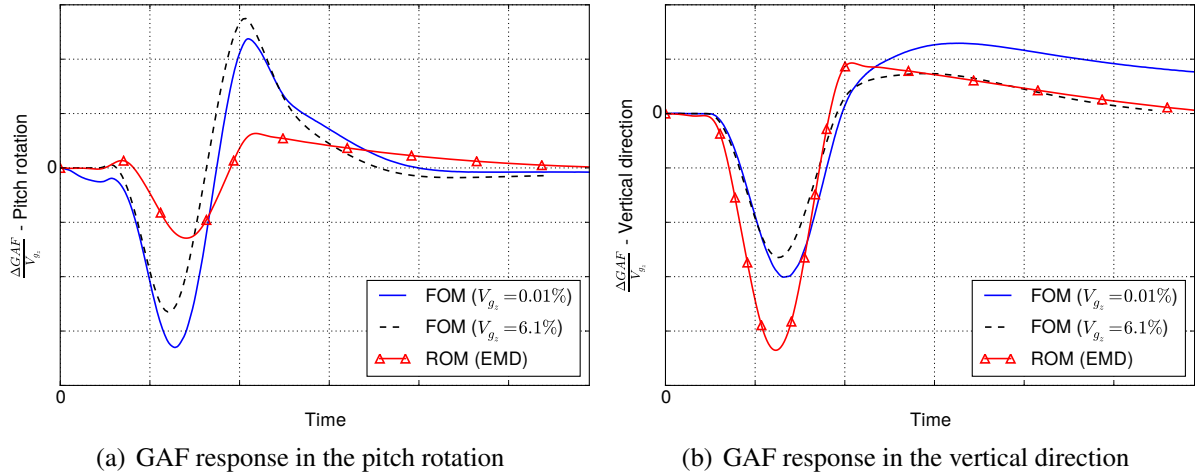
11

(a) GAF response in the pitch rotation   (b) GAF response in the vertical direction

Figure 7: Response to '1-cos' gust with wavelength $L_g = 116$ m and gust amplitudes $V_{g_z} = 0.01\%$ and $V_{g_z} = 6.1\%$ of free-stream velocity. ROM includes flight dynamics modes only.

the large amplitude gust. An offset between linear and regulation gusts is visible at the end of the simulation. This depends on the tiny amplitude used for the linear excitation whose effects are dissipated more quickly. The full order results are compared to the ROM which shows some discrepancies in the peak values and a phase lag. This is due to a lack of information to fully reconstruct the effect of aerodynamic disturbances. The flight dynamics eigenvectors, coming from the Jacobian matrix of the coupled system, are unable to fully account for the effects of pure aerodynamic disturbances such as gusts. When the gust has passed the aircraft, the reduced model converges to the full order results. This behaviour is confirmed by the vertical GAF in Fig. 7(b). The first peak, which is mainly due to the aerodynamic disturbance, is not fully predicted. Thereafter, the GAF value provided by the reduced model converges to the reference value confirming that flight dynamics modes are able to describe the system behaviour when not subject to external disturbances.

The snapshot method was investigated to overcome this problem. A snapshot matrix is populated with 20 solutions to Eq. (9) and their complex-conjugates, each corresponding to a harmonic fluid response for a sinusoidal gust in the reduced frequency range $[0, 2]$. POD decomposition was applied to obtain 40 POD modes which describe the aerodynamic response. Considering a static aircraft, i.e. neither moving in the longitudinal nor lateral degrees-of-freedom, the reduced model containing POD modes only is capable of reproducing the full order results as presented in Fig. 8 for a '1-cos' gust with amplitude $V_{g_z} = 0.01\%$ of free-stream velocity and gust length $L_g = 116$ m. Regarding the lift coefficient in Fig. 8(a), full order results are characterised by a peak value followed by a smooth decay. The reduced model follows the reference curve and peak values as well as transient behaviour are well reproduced. A similar trend is shown for the moment coefficient in Fig. 8(b) which is evaluated accurately by the reduced model, confirming that the reduction with POD modes is a valid approach for the static case.

The POD modes were used for the free-flight problem by adding them to the modal bases Φ and Ψ in Eq. (10). These are now composed of flight dynamics modes identified with the operator-based method and POD modes as specified in Eq. (23). Approximate eigenvalues of A were obtained by calculating the eigenvalues of the reduced matrix $\Psi^H A \Phi$ and results are shown in Fig. 9. A comparison with flight dynamics eigenvalues calculated with the operator-based identification shows that eigenvalues related to flight dynamics are affected by the coupling since they move slightly in terms of both frequency and damping. Approximate eigenvalues of

(a) Variation of the lift coefficient
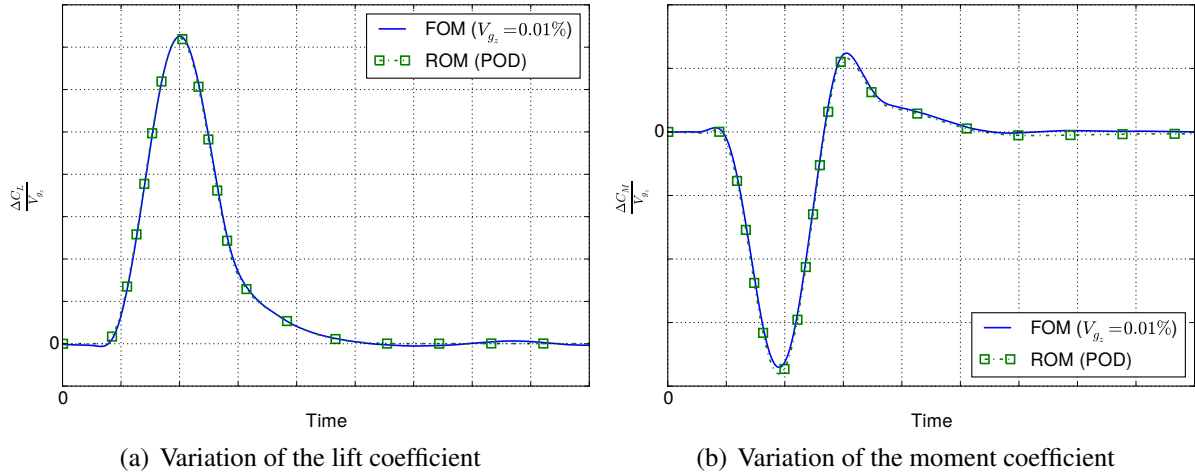
(b) Variation of the moment coefficient

Figure 8: Response to '1-cos' gust with wavelength $L_g = 116$ m and gust amplitude $V_{g_z} = 0.01\%$ of free-stream velocity for a fixed aircraft. ROM includes POD modes only.
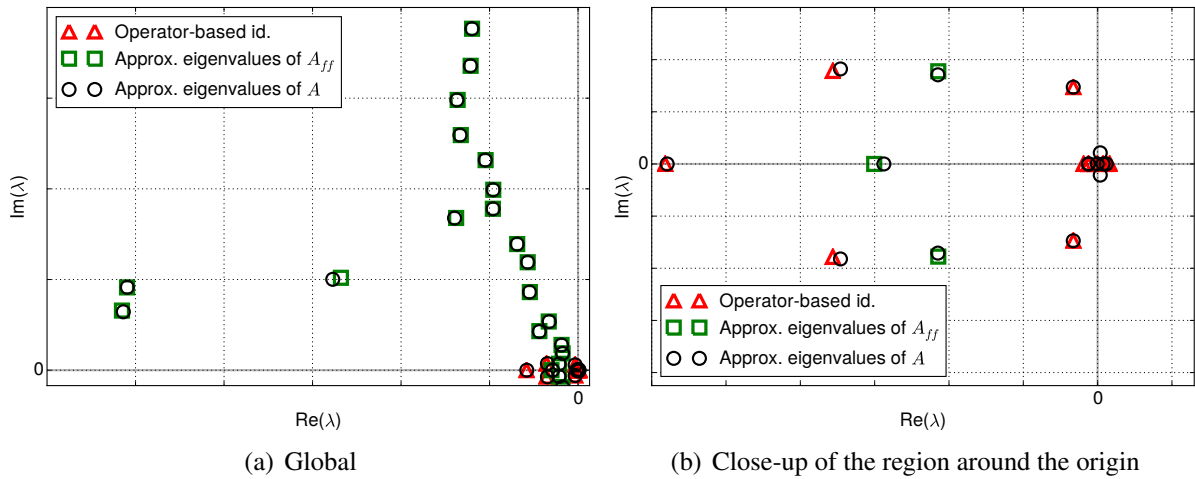

(a) Global

(b) Close-up of the region around the origin

Figure 9: Eigenspectrum comparing approximate eigenvalues calculated with the operator-based identification, POD and joint approaches.

A_{ff} were obtained solving the eigenproblem for $\Psi_{\text{POD}}^H A_{ff} \Phi_{\text{POD}}$ and they are reported in Fig. 9 as well. Their locations in the complex plane change when flight dynamics modes are added. Negative imaginary parts in the global view are omitted to increase visibility.

The reduced model based on flight dynamics and POD modes was used to simulate an encounter with a '1-cos' gust with amplitude $V_{g_z} = 0.01\%$ of free-stream velocity and gust length $L_g = 116$ m. Results are presented in Fig. 10 together with the ones obtained using flight dynamics modes only. Figure 10(a) shows a very good agreement between the full order model and ROM using flight dynamics and POD modes for pitch rotation GAF. The general trend is well represented and results match after the disturbance has passed the aircraft. Peak values are also well reproduced with a minor error on the first peak. The ROM behaviour is confirmed for the vertical GAF in Fig. 10(b) since the reference data is accurately reproduced.

Regarding the cost of building the reduced model, it can be split in two parts. The first is given by the operator-based identification which required the calculation of 7 GAF matrices for a total of 42 LFD solves for columns of A_{fs}. A number of 18 additional solutions are needed to obtain the direct and adjoint eigenvectors. The second part involves the evaluation of POD modes with

(a) GAF response in the pitch rotation
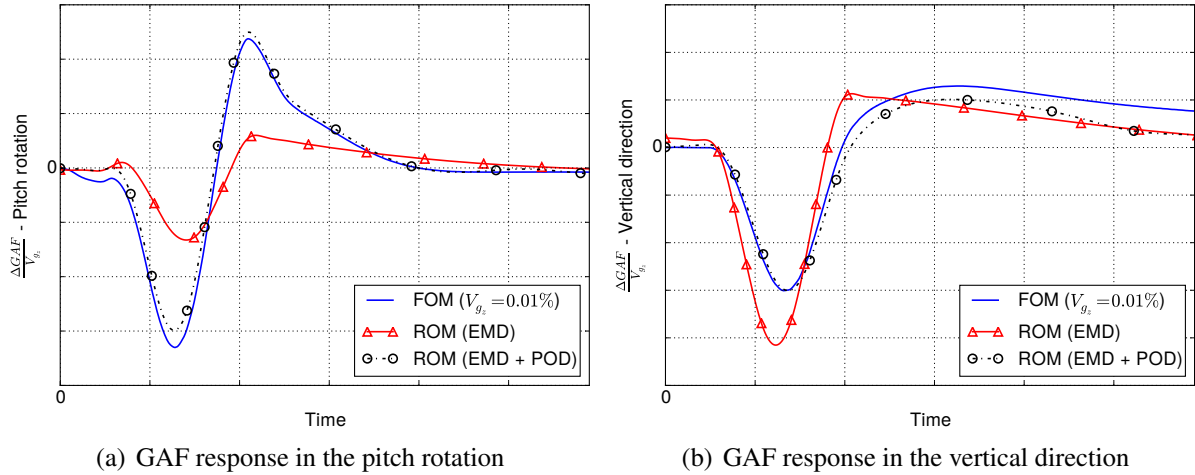
(b) GAF response in the vertical direction

Figure 10: Response to '1-cos' gust with wavelength $L_g = 116$ m and gust amplitude $V_{g_z} = 0.01\%$ of free-stream velocity. ROM includes flight dynamics and POD modes.
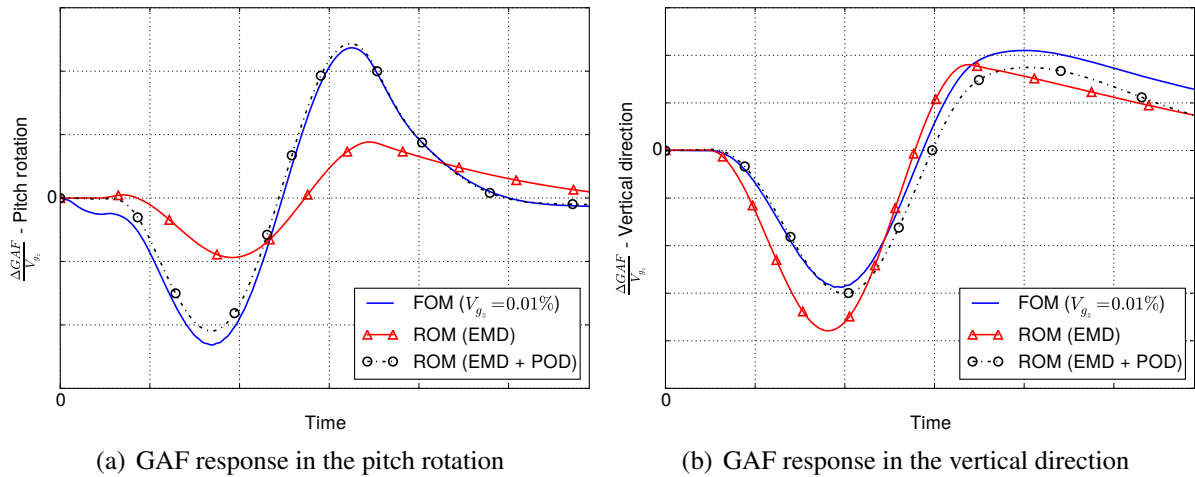

(a) GAF response in the pitch rotation

(b) GAF response in the vertical direction

Figure 11: Response to '1-cos' gust with wavelength $L_g = 214$ m and gust amplitude $V_{g_z} = 0.01\%$ of free-stream velocity. ROM includes flight dynamics and POD modes.

20 solutions of Eq. (9). The total cost of the ROM is estimated in 80 LFD computations. The cost of a single full order simulation is comparable to 48 LFD solves using the same hardware configuration. However, it is empathised here that multiple gust lengths must be investigated during the aircraft design and certification procedure, and each one requires an individual full order simulation. Conversely, the reduced model can be used to simulate encounter with gusts having different lengths, each at a negligible computational cost, as shown in Fig. 11 for a '1-cos' gust with length $L_g = 214$ m and amplitude $V_{g_z} = 0.01\%$ of free-stream velocity. Using only flight dynamics modes for the reduction leads to inaccurate results for the peak values, as already presented for the shorter gust. However, the enhanced reduced model matches the reference in terms of transient response as well as peak values for pitch rotation GAF as depicted in Fig. 11(a). Similar results are reported for the vertical direction GAF in Fig. 11(b). This confirms that the model reduction technique is a valid tool to evaluate the response of free-flying aircraft subject to gust disturbances.

5 CONCLUSIONS

The work describes the development and application of a model reduction technique for coupled simulations involving flight dynamics and computational fluid dynamics. Model reduction is achieved by projecting the Taylor-expanded full order coupled non-linear residual function onto a modal basis populated with eigenvectors of the coupled system. An operator-based modal identification technique is adopted as procedure to obtain eigenvectors from the coupled Jacobian matrix related to flight dynamics degrees-of-freedom. This method is suitable for large test cases since it does not rely on the direct calculation of the system's eigenspectrum. An exact formulation is provided with the Schur complement method and an approximation, using a pre-computation of interaction terms, is used as trade-off between computational cost and accuracy. Operator-based identification provides modes suitable to represent the behaviour of the system not subject to any external disturbance, resulting in a versatile model which can be easily exploited for stability analysis. Extending this technique for external disturbances such as gusts requires additional modes describing the aerodynamic response. These are obtained by sampling the fluid response subject to sinusoidal gust excitations and applying proper orthogonal decomposition. Those resulting modes are then combined together with the eigenpairs from the operator-based identification in the same modal basis to perform gust encounter simulations of free-flying aircraft.

The method is applied to a large civil aircraft in the transonic regime. The problem is investigated for a rigid aircraft. Flight dynamics eigenpairs evolve from in-vacuum rigid body modes and the corresponding eigenvalues move from the origin to new positions as shown with part of the eigenspectrum. The reduced model including flight dynamics modes only is capable of reproducing full order results for initial disturbance analysis but produces inaccurate results for gust encounter. The enhanced reduced model on the other hand, which contains modes related to the aerodynamic subsystem, provides an accurate solution for gust simulations. Overall, the reduced model is capable of reproducing full order results for initial disturbance and multiple gust lengths at a fraction of the computational cost.

Future development will focus on including elastic modes into the reduced model to add structural flexibility effects. The technique will then be applied to free-flying flexible aircraft subject to gust disturbances. In addition, applications of this method will target lateral gusts to fully exploit the three-dimensional flight dynamic model.

ACKNOWLEDGEMENTS

6 REFERENCES

[1] Slotnick, J., Khodadoust, A., Alonso, J., et al. (2013). CFD vision 2030 study: a path to revolutionary computational aerosciences. Tech. Rep. NASA/CR-2014-218178, NASA Langley Research Center.

[2] EASA (2007). Certification specifications and acceptable means of compliance for large aeroplanes CS-25 amendment 15.

[3] Cook, R. G. and Palacios, R. (2013). Robust gust alleviation and stabilization of very flexible aircraft. *AIAA Journal*, 51(2), 330–340.

[4] Ricciardi, A. P., Patil, M. J., and Canfield, R. A. (2013). Evaluation of quasi-static gust loads certification methods for high-altitude long-endurance aircraft. *Journal of Aircraft*, 50(2), 457–468.

[5] Raveh, D. E. and Karpel, M. (2000). Nonlinear design loads for maneuvering elastic aircraft. *Journal of aircraft*, 37(2), 313–318.

[6] Reimer, L., Ritter, M., Heinrich, R., et al. (2015). CFD-based gust load analysis for a free-flying flexible passenger aircraft in comparison to a DLM-based approach. AIAA-2015-2455.

[7] Bekemeyer, P., Thormann, R., and Timme, S. (2017). Frequency-domain gust response simulation using computational fluid dynamics. *AIAA Journal*. Accepted for publication.

[8] Badcock, K., Timme, S., Marques, S., et al. (2011). Transonic aeroelastic simulation for instability searches and uncertainty analysis. *Progress in Aerospace Sciences*, 47(5), 392–423.

[9] Timme, S., Badcock, K. J., and Da Ronch, A. (2013). Linear reduced order modelling for gust response analysis using the DLR-TAU code. IFASD-2013-36A.

[10] Stroscher, F., Sika, Z., and Petersson, O. (2013). Reduced order model of a blended wing body aircraft configuration. *Progress in Flight Dynamics*, 6, 635–650.

[11] Da Ronch, A., Badcock, K. J., Wang, Y., et al. (2012). Nonlinear model reduction for flexible aircraft control design. AIAA 2012-4404.

[12] Da Ronch, A., Tantaroudas, N., Timme, S., et al. (2013). Model reduction for linear and nonlinear gust loads analysis. AIAA-2013-1492.

[13] Timme, S., Marques, S., and Badcock, K. J. (2011). Transonic aeroelastic stability analysis using a Kriging-based Schur complement formulation. *AIAA Journal*, 49(6), 1202–1213.

[14] Pagliuca, G. and Timme, S. (2016). Flight dynamics mode identification and model reduction using computational fluid dynamics. AIAA-2016-3850.

[15] Gai, G. and Timme, S. (2016). Nonlinear reduced-order modelling for limit-cycle oscillation analysis. *Nonlinear Dynamics*, 84, 991–1009.

[16] Woodgate, M. A. and Badcock, K. J. (2007). Fast prediction of transonic aeroelastic stability and limit cycles. *AIAA Journal*, 45(6), 1370–1381.

[17] Bekemeyer, P. and Timme, S. (2016). Reduced order gust response simulation using computational fluid dynamics. AIAA-2016-36A.

[18] Bekemeyer, P. and Timme, S. (2017). Reduced order transonic aeroelastic gust response simulation of large aircraft. AIAA-2017-4361.

[19] Wright, J. and Cooper, J. (2007). *Introduction to aircraft aeroelasticity and loads*. Wiley.

[20] Cook, M. (2007). *Flight Dynamics Principles*. Elsevier.

[21] Meinel, M. and Einarsson, G. (2010). The FlowSimulator framework for massively parallel CFD applications. In *Para 2010 - State of the Art in Scientific and Parallel Computing*, PARA2010-44.

[22] Xu, S., Timme, S., and Badcock, K. (2016). Enabling off-design linearised aerodynamics analysis using krylov subspace recycling technique. *Computer and Fluids*, 140, 385–396.

[23] Rodden, W. and Giesing, J. P. (1970). Application of oscillatory aerodynamic theory to estimation of dynamic stability derivatives. *Journal of Aircraft*, 7(3), 272–275.

[24] Da Ronch, A., Vallespin, D., Ghoreyshi, M., et al. (2012). Evaluation of dynamic derivatives using computational fluid dynamics. *AIAA Journal*, 50(2), 470–484.

[25] Hassig, H. (1971). An approximate true damping solution of the flutter equation by determinant iteration. *Journal of Aircraft*, 8, 885–889.

[26] Sirovich, L. (1987). Turbulence and the dynamics of coherent structures, Parts I-III. *Quarterly of Applied Mathematics*, 45(3), 561–590.

[27] Bekemeyer, P., Thormann, R., and Timme, S. (2016). Rapid gust response simulation of large civil aircraft using computational fluid dynamics. In *Royal Aeronautical Society - Applied Aerodynamics Conference*.

[28] Schwamborn, D., Gerhold, T., and Heinrich, R. (2006). The DLR-TAU code: recent applications in research and industry. In *European Conference on Computational Fluid Dynamics*.

[29] Stickan, B., Dillinger, J., and Schewe, G. (2014). Computational aeroelastic investigation of a transonic limit-cycle-oscillation experiment at a transport aircraft wing model. *Journal of Fluids and Structures*, 49, 223–241.

[30] Neumann, J. and Mai, H. (2013). Gust response: simulation of an aeroelastic experiment by a fluid-structure interaction mehod. *Journal of Fluids and Structure*, 38, 290–302.

[31] Spalart, P. and Allmaras, S. (1994). A one equation turbolence model for aerodynamic flows. *Recherche Aerospatiale*, 1, 5–21.

[32] Jamenson, A., Schmidt, W., and Turkel, E. (1981). Numerical solutions of the Euler equations by finite volume methods using Runge-Kutta time-stepping schemes. AIAA-1981-1259.

[33] Dwight, R. (2006). An implicit LU-SGS scheme for finite-volume discretizations of the Navier-Stokes equations on hybrid grids. DLR-FB-2005-05.

[34] Heinrich, R. and Reimer, L. (2013). Comparison of different approaches for gust modeling in the CFD code TAU. IFASD-2013-36B.

[35] Newmark, N. (1959). A method of computation for structural dynamics. *Journal of Engineering Mechanics*, 85(3), 67–94.

[36] de Boer, A., van der Schoot M.S., and Bijl, H. (2007). Mesh deformation based on radial basis function interpolation. *Computers and Structures*, 85(11-14), 784–795.

[37] Roskam, J. (1995). *Airplane flight dynamics and automatic flight controls*. DARcorporation.

[38] Broyden, C. (1965). A class of methods for solving nonlinear simultaneous equations. *Mathematics of Computation*, 19, 577–593.

[39] Bisplinghoff, R., Ashley, H., and Halfman, R. (1955). *Aeroelasticity*. Addison-Wesley.

COPYRIGHT STATEMENT